Geometry of fully coordinated, two-dimensional percolation

E. Cuansing, J. H. Kim* and H. Nakanishi
Department of Physics, Purdue University, West Lafayette, Indiana 47907
(Received 21 April 1999)

We study the geometry of the critical clusters in fully coordinated percolation on the square lattice. By Monte Carlo simulations (static exponents) and normal mode analysis (dynamic exponents), we find that this problem is in the same universality class with ordinary percolation *statically* but not so *dynamically*. We show that there are large differences in the number and distribution of the *interior* sites between the two problems that may account for the different dynamic nature. [S1063-651X(99)04610-3]

PACS number(s): 05.40.Fb, 05.70.Fh, 05.70.Jk, 64.60.Ak

I. INTRODUCTION

The geometrical phase transition known as percolation (see, for a review, Stauffer and Aharony [1]) is appreciated by many to be an elegant and simply defined yet fully featured example of a second order phase transition. A number of variations of the original percolation problem were proposed as better models of some physical phenomena in the past. This includes the *backbone* percolation for studying electrical conduction through random media, *polychromatic* percolation for multicomponent composites, and *fourfold coordinated* bond percolation for hydrogen-bonded water molecules. In particular, Blumberg *et al.* [2] and Gonzalez and Reynolds [3] studied a random bond, site-correlated percolation problem they call four-coordinated percolation on the square lattice. They conclude that this problem belongs to the same universality class as the ordinary random percolation with the same set of (static) exponents.

In this paper, we revisit a problem in this realm, though not exactly the same one. We define *fully coordinated percolation* as the site percolation problem where only the occupied sites all of whose neighboring sites are also occupied can transmit connectivity. Since the random element is the site, this problem is slightly different from the bond problem referred to above. Thus, after generating a random site configuration with the independent site occupation probability p, we only select those occupied sites with all four neighbors also occupied on the square lattice and study the clusters formed by nearest neighbor connections among those sites. It should be noted that this problem is distinct from the so-called bootstrap percolation (see, e.g., [4]) where sites of less connectivity are iteratively removed. In our problem, no iterative procedures are involved; rather, sites of less than full connectivity are marked first and then all of them removed at one time.

This problem arose in the context of studying the vibrational properties of fractal structures tethered at their boundaries [5,6]. In that problem, scaling was observed in the normal mode spectrum whose origin may lie in the ratio of two length scales, one of which is the size of highly connected regions of a cluster. In this context, we have embarked on revisiting the characteristics of randomly generated but highly connected geometrical structures.

In the next section, we summarize the Monte Carlo and finite size scaling analyses of the static critical properties of fully coordinated percolation. In Sec. III, we discuss the normal modes of the *transition probability matrix* for tracer diffusion on the structure using the methods of Arnoldi and Saad (see, e.g., [8]). Then in Sec. IV, we describe the classification of the cluster sites into external boundary, internal boundary, and interior ones and use these to show the major distinctions between the critical clusters of ordinary and fully coordinated percolation. We summarize the results in the final section.

II. STATIC CRITICAL BEHAVIOR

To determine the static critical behavior of fully coordinated percolation we first performed Monte Carlo simulations on a square lattice in two dimensions. Each site is occupied with probability p independently and subsequent fully coordinated sites are marked and their connectivity searched. Lattice sizes of L^2 where $L=256$, 512, 1024, and 2048 were constructed. For each lattice size we further made a thousand realizations wherein a different random number seed was used on every run. The unnormalized susceptibilities, i.e., $\Xi(L)=\Sigma_s' s^2 \hat{n}_s$ where $\hat{n}_s$ is the number of clusters of size s, are calculated on each run and are then summed at the end of the thousand realizations. The average susceptibilities χ are calculated by dividing the sum by the number of realizations and the lattice size. The prime on the summation indicates the fact that the contribution of the largest cluster to χ near and above what we perceived to be the critical probability p_c has been subtracted as usual [1].

In Fig. 1 we plot the average susceptibilities against the probability p for the corresponding lattice sizes. The data correspond to the values of $L=256$, 512, 1024, and 2048 from the lowest to highest. We can see that the effects due to the finite sizes of the lattices are exhibited clearly. In particular, there are well-defined peaks which scale with lattice sizes as

$$\chi(p_{max},L)\sim L^{\gamma/\nu}, \tag{1}$$

where the known exact value of γ/ν for the ordinary percolation is $\frac{43}{24}\sim 1.7917$. To demonstrate the precision of our

*Present address: Department of Physics, Kangnung National University, Kangnung, Kangwon 210-702, South Korea.

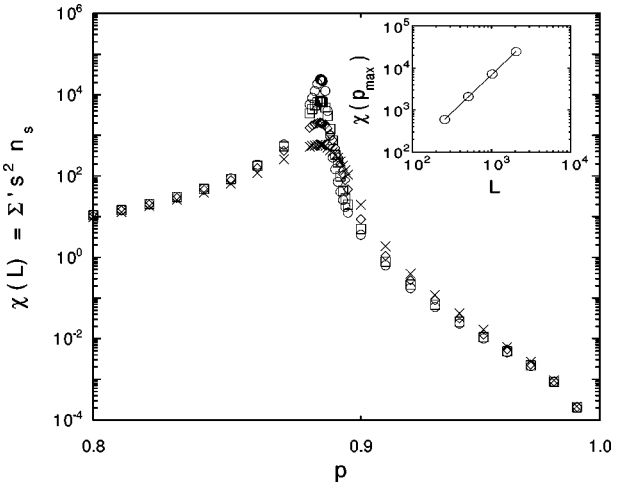

FIG. 1. Susceptibilities χ for fully coordinated percolation on finite square lattices of size L^2 are shown against probability p, where crosses, diamonds, squares, and circles are for $L=256, 512, 1024$, and 2048, respectively. The inset shows the finite-size scaling of the peaks of these curves by plotting the maximum χ vs L on a log-log scale. L is a dimensionless quantity corresponding to the length, in multiples of the lattice constant, of the side of a square lattice.

calculations, we plot $\chi(p_{max},L)$ against the corresponding lattice sizes in the inset of Fig. 1. Notice that the data follow an excellent power law, leading to a least squares fit of $\chi(p_{max},L)\sim L^{1.7911}$. The value of γ found is identical to the ordinary percolation value to within about 0.03%. This result confirms previous work [2,3] stating that fully coordinated percolation and ordinary percolation belong to the same *static* universality class.

The critical behavior of susceptibility is known to scale as [1]

$$\chi(p,\infty)\sim|p-p_c|^{-\gamma}, \tag{2}$$

where for ordinary percolation $\gamma_o=\frac{43}{18}\sim 2.3889$. Notice, however, that in Fig. 1 the peaks are very near $p=1.0$. This would provide data to the right of the peaks in only a small probability interval. In our simulations, we would therefore use χ only to the left of the peaks.

Since the scaling relation in Eq. (2) is expected only for infinite lattices, we use only the data taken from $L=2048$ to test it. Since there are two unknowns in Eq. (2), we first choose a particular p_c and make a fit to see what value of γ_{exp} is obtained. If we choose $p_c=0.886$ we get $\gamma_{exp}=2.4004$. The correlation coefficient, $|R|$, for this fit is 0.999 99. The discrepancy between γ_{exp} and γ_o is around 0.481%. Choosing $p_c=0.8858$ we obtain $\gamma_{exp}=2.3864$. The discrepancy this time is around 0.10% and $|R|=1$. So we have an exact fit for this value of p_c and the γ_{exp} found is very close to the γ_o. Choosing $p_c=0.885$ we obtain $\gamma_{exp}=2.3302$ with an $|R|=0.999\,99$. The discrepancy for this value of p_c is 2.46%. Fits done with p_c between 0.885 and 0.886 gave $|R|=1$; however, the γ_{exp} found when $p_c=0.8858$ gave the closest value to γ_o. This allows us to conclude that γ for fully coordinated percolation is the same as that for ordinary percolation while also giving an estimate for the value of p_c close to 0.8858. (We will state the experimental uncertainty for p_c after all our analyses are presented.)

From the fit done to examine the scaling in Eq. (1) we could further conclude that ν for fully coordinated percolation should be the same with that for ordinary percolation. This again confirms the statement that fully coordinated percolation is in the same *static* universality class as ordinary percolation. Another universal constant often used to characterize ordinary percolation is the amplitude ratio C_+/C_- of susceptibility χ (whose value is about 200 in $d=2$ [7]). In fully coordinated percolation, this quantity is unfortunately difficult to calculate accurately because the critical region for $p>p_c$ is very small (see below). When we constrain the exponent γ to be close to γ_o and use the p_c estimated in this work, however, we find that C_+/C_- is of $\mathcal{O}(10^2)$, which is consistent with the above observation as well.

The contribution of the largest cluster to the susceptibility is not significant when $p<p_c$. However, when $p\sim p_c$ a significant number of sites will belong to the largest cluster and when $p>p_c$ the largest cluster is dominant in the whole lattice. The average susceptibility contribution due to this largest cluster is $\chi_1=\Sigma s_{max}^2/(L^2N)$, where the summation is over $N=1000$ realizations and s_{max} is the size of the largest cluster. The fractal dimension, d_f, can be obtained from s_{max} by

$$s_{max}(p_c)\sim L^{d_f}, \tag{3}$$

where $\overline{s_{max}}(p_c)$ is the mean size of the largest cluster at p_c. χ_1 should therefore scale as

$$\chi_1\sim L^{2d_f-2}. \tag{4}$$

For ordinary percolation on a two dimensional lattice (see, e.g., [1]), it is known that $d_f=91/48$ and $y\equiv 2d_f-2\sim 1.7917$. For fully coordinated percolation, the scaling in Eq. (4) have two unknowns, p_c and d_f. Similarly to what we have done when examining the scaling in Eq. (2), we choose trial values for p_c and then perform a least squares fit to obtain the corresponding $y=2d_f-2$. By looking for the range of trial p_c that maximizes the regression coefficient $|R|$, we arrive at an estimate of p_c to be close to 0.8845, where $|R|=1$ and $y=1.7855$. The variation of $|R|$ is about two parts in 10^5 if p_c is varied by 0.0002, always with less than 1% deviation from the ordinary percolation value of y. From these results we conclude that d_f for fully coordinated percolation is the same as that for ordinary percolation as well as the estimate of about 0.8845 for p_c.

In addition to the above, we have also performed the scaling analysis of the quantity $\chi_1(p,L)$, as both p and L are varied, in the form of

$$\chi_{i1}=L^{2d_f-2}g(|p-p_c|^{\nu}L), \tag{5}$$

where $g(|p-p_c|^{\nu}L)$ is a scaling function. Using the exactly known ordinary percolation values of the exponents d_f and ν (as they have been shown to be the same for fully coordinated percolation above), we obtained the maximum data collapsing in the range of $0.884<p_c<0.885$.

Independent of the above analyses based on the fully coordinated clusters obtained by Monte Carlo simulations of

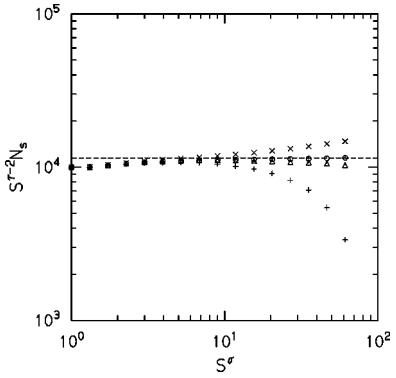

FIG. 2. The scaled partial sum N_s is plotted against s^σ for $p=0.890$ (crosses), 0.885 (circles), 0.884 (triangles), and 0.880 (plusses). The dashed line is a horizontal line to guide the eye, showing that the data for $p=0.885$ best fits the horizontal slope for large cluster sizes.

fixed-sized square grids, we have also performed Monte Carlo simulations by growing fully coordinated clusters starting from a seed site using a variant of the *breadth-first search* algorithm [8]. This latter approach has an advantage that there is no obvious finite-size effects and that statistics taken while a cluster is still growing represents a *partial sum* automatically. That is, we start growing such clusters 10 000 times at each of $p=0.880$, 0.884, 0.885, and 0.890, and keep track of how many of them are still growing at predetermined intervals of size (2^n where $n=1,2,\ldots,15$ in our case). This number, say, N_s represents the partial sum

$$N_s/N_1=\frac{1}{p}\sum_{s'\geqslant s} s' n_{s'}. \tag{6}$$

Since the normalized number of size-s clusters, n_s, scales as $s^{-\tau}f(\epsilon s^\sigma)$, where $\tau=187/91$ and $\sigma=36/91$, we expect that N_s scales as

$$N_s s^{\tau-2}\sim \hat{f}(\epsilon s^\sigma) \tag{7}$$

near p_c and for large s. In particular, at p_c, this quantity should be constant independent of (large) s. The numerical results are shown in Fig. 2, where the data correspond, from highest to lowest, to $p=0.890$, 0.885, 0.884, and 0.880. The horizontal dashed line drawn to guide the eye makes it clear that data for $p=0.885$ best approximates a horizontal line as $s\to\infty$, suggesting that a good estimate of p_c would be 0.885.

We now consider all the above results together. The results from scaling in Eq. (2) indicate a range 0.885–0.886, and those from scaling in Eq. (4) indicate 0.8844–0.8847, while those from scaling in Eq. (5) hints at p_c being in the 0.884–0.885 interval. Another result that could also be used are the values of p for the peaks in Fig. 1, which vary from 0.8841 to 0.8844 (with the peak for the largest grid $L=2048$ occurring at $p_{peak}=0.8844$). Combining all these results, our final estimate is $p_c=0.885\pm0.001$.

III. DYNAMIC CRITICAL BEHAVIOR

By dynamic critical behavior here we simply mean the asymptotic long-time behavior of diffusion taking place on an incipient infinite cluster of fully coordinated percolation, or its equivalent *scalar* elastic behavior. This represents the simplest kind of dynamics associated with these complicated geometrical objects and is mainly reflected in the two *dynamic* critical exponents called d_s (spectral dimension) and d_w (walk dimension).

It is well known (see, e.g., [10]) that the return-to-the starting point probability of the random walk, $P(t)$, in the long-time limit obeys the power law

$$P(t)\sim t^{-d_s/2}, \tag{8}$$

where d_s is the spectral dimension of the walk. In a fractal medium, d_s is less than the space dimension d, because the progressive displacement of the random walker further from the starting point is hampered by its encounter with the irregularities of the medium at all scales. Thus, d_s is expected to be greater for environments that provide higher connectivity at large length scales, independently of the fractal dimension itself which is mainly the measure of the overall *size* scales or *how many* sites are connected, not *how well* those sites are connected to each other.

For media with long-range loops, d_f (fractal dimension), d_s, and d_w are not independent but are expected to obey the well-known Alexander and Orbach scaling law [10]

$$d_s=2d_f/d_w. \tag{9}$$

For this reason, we only calculate d_s here though both d_s and d_w can be conveniently calculated by numerically studying the *transition probability matrix* **W** which represent the random walk on a specific fractal medium. Our calculation in this work is only one aspect of such an analysis: finite size scaling of the dominant nontrivial eigenvalue which describes the longest finite time scale of the Brownian process. This approach has already been described in detail elsewhere [9], and thus we merely state the main feature and then immediately report our specific numerical results.

The matrix **W** is constructed from the elements W_{ij} being equal to a hopping probability per step (equal to $\frac{1}{4}$ here) for available nearest neighbor sites i and j. For each neighbor site which is not present, a probability of $\frac{1}{4}$ is added to the probability for not taking a step for one time period; this is called the *blind ant* rule. Many large matrices **W** are obtained by Monte Carlo simulation (by growing a fully coordinated percolation cluster from a seed site and stopping the growth when a predetermined desired size is reached) and their largest eigenvalues are numerically obtained by the so-called *Arnoldi-Saad* method. The dominant nontrivial eigenvalue λ_1 is the largest eigenvalue just below the stationary eigenvalue 1 and it is known to satisfy the following finite size scaling law:

$$|\ln\lambda_1|\approx 1-\lambda_1\sim S^{-2/d_s}. \tag{10}$$

Shown in Fig. 3 are our results from such an analysis. We have generated at least 1000 independent realizations of the underlying fully coordinated percolation clusters for sizes $S=1250$, 2500, 5000, 10 000, and 20 000 at each of the three nominal probabilities $p=0.883$, 0.885, and 0.887, and numerically obtained λ_1 for each cluster. The main part of Fig. 3 shows the data from $p=0.885$, the value shown to be closest to p_c in this work. The figure shows an excellent power

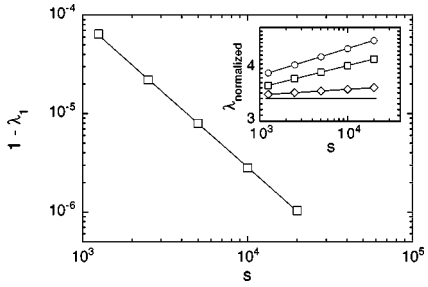

FIG. 3. The scaling of the largest nontrivial eigenvalue λ_1 of the Markov chain analysis is shown by plotting $1-\lambda_1$ against the cluster size s on a log-log scale. The inset shows a normalized λ (see text) for $p=0.887$, 0.885, and 0.883 (from top). The solid line is horizontal, corresponding to the slope for ordinary percolation.

law fit (regression coefficient of $-0.999\,93$) to Eq. (10) with the exponent $2/d_s=1.486\pm0.01$. This power translates to $d_s=1.346\pm0.011$, which is close to but significantly larger than the corresponding ordinary percolation value of $d_s^{(O)}=1.30\pm0.02$ estimated by many independent calculations. (See, e.g., [8].) For comparison, a *loopless* variant of percolation has exactly the same static exponents as ordinary percolation but has $d_s\approx1.22$ in two dimensions, about twice as much deviation from ordinary percolation in the opposite direction as the present fully coordinated percolation problem [11].

In the inset for Fig. 3, we show a normalized λ_1 by plotting $(1-\lambda_1)S^{2/d_s^{(o)}}$, where the circles are for $p=0.887$, squares for $p=0.885$, diamonds for $p=0.883$, and the solid line is a horizontal line (for ordinary percolation) to guide the eye. In all cases, the standard errors of the mean for each set of data are substantially smaller than the size of the symbols used in the figure. The distribution of λ_1 in each case appears to be Gaussian with the standard deviations scaling in the same way as the means.

From these results, we conclude that, though the numerical differences are small, it is likely that the fully coordinated percolation clusters are significantly different from the ordinary percolation counterparts even at long length scales. In the next section, we show that this analysis is vindicated by exposing one dramatic difference in the cluster morphology which will not be obvious to an uncritical observer.

IV. CLUSTER GEOMETRY

In this section we examine the geometry of fully coordinated percolation clusters more closely. First, we present Fig. 4 which show in gray scale the sites of (a) fully coordinated percolation cluster and (b) ordinary percolation cluster at respective p_c. The overall visual impression is that they are very similarly shaped even down to the details of the boundaries and internal holes. Their shapes are also essentially independent of the underlying lattice anisotropy. However, the number and distributions of the especially dark points are evidently quite distinct in Fig. 4(a) and 4(b). They cluster more and are much more abundant in Fig. 4(a) than in 4(b). These sites are actually the *interior* or fully coordinated sites in the internal part of the cluster. The remaining sites (shaded gray) are either the external *hull* sites or internal boundary sites.

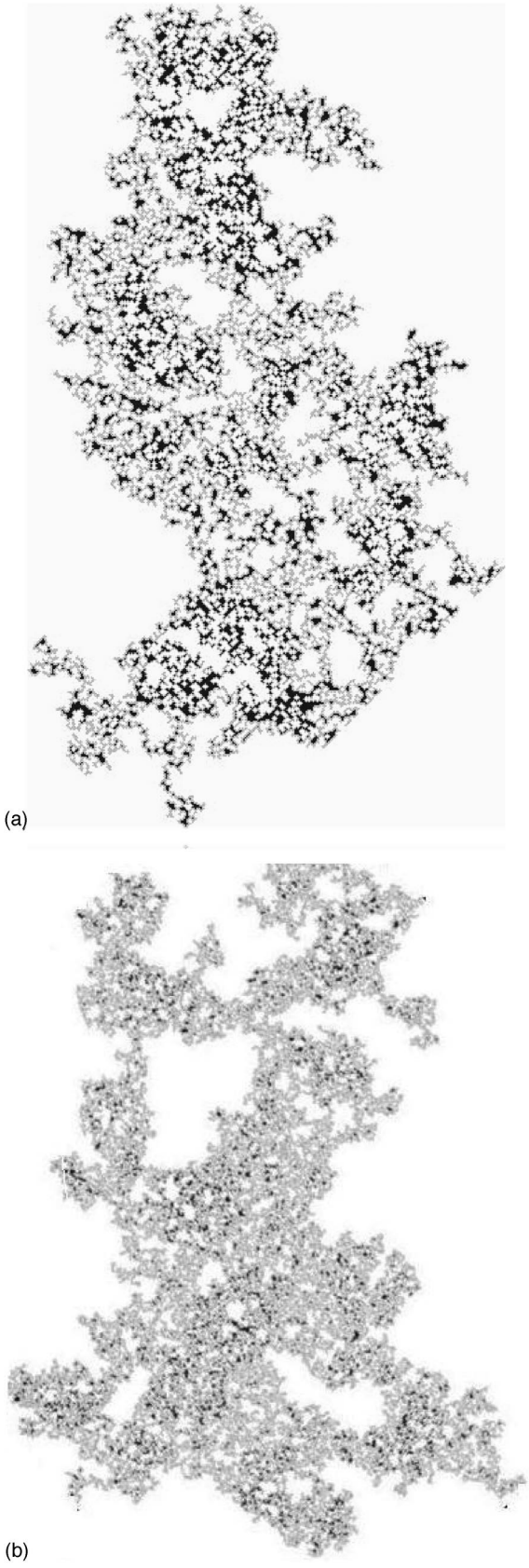

FIG. 4. (a) A typical fully coordinated percolation cluster at its p_c, and (b) the corresponding critical ordinary percolation cluster. The dark points are the *interior* sites of full coordination and the gray shaded sites are either on the external hull or internal boundaries.

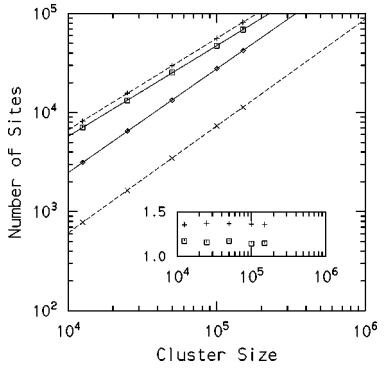

FIG. 5. The numbers of *external* sites (squares and plusses) and those of *interior* sites (diamonds and crosses) are scaled against the cluster size s. The solid (fully coordinated percolation) and dashed (ordinary percolation) lines are the linear least squares fits. In the inset, we show the number of external sites divided by $s^{d_h^{(o)}/d_f^{(o)}}$, showing that the population of the external *hull* sites of fully coordinated and ordinary percolation scale in the same way.

In Fig. 5 quantitative examination is made on the different classes of sites of the two kinds of clusters. In the main part of the figure, the average numbers of two kinds of sites are shown, *interior* (diamonds for fully coordinated percolation, crosses for ordinary percolation), and *external* (squares for fully coordinated percolation, pluses for ordinary percolation). It is clear that the interior sites are more than three times more abundant in fully coordinated percolation, than in ordinary percolation as is visually suggested by Fig. 4. Though this is primarily a local effect due to the full coordination rule, they do have a multiplicative effect at long-range connectivity and thus may well be the source of the small difference in the value of d_s.

Of course just the fact that there are more than three times as many interior sites (and correspondingly, much fewer *hull* sites) in fully coordinated percolation must have quantitative consequences (even if not qualitative) for any process on the cluster which depends on degrees of connectivity rather than just on the number of connected sites. An example of the effect of the different numbers of the hull sites may be in oxidation or catalysis of a material through the external embedding phase or even a irregularly shaped breakwater in the form of the external boundary of a percolation cluster. The *external* sites are those which are sometimes called *hull* sites, and they are known to scale with an exact exponent in ordinary percolation as

$$N_{hull} \sim S^{d_h/d_f}, \tag{11}$$

where $d_h^{(o)} = 7/4$ and thus the exponent is $84/91 = 0.923\ldots$ for ordinary percolation. Since this is less than 1, these sites comprise less and less of the cluster as $s \to \infty$ and the remaining sites (i.e., *interior* and *internal boundary* sites) eventually dominate the whole cluster. This is already evident from the greater slopes close to 1 for the *interior* sites in Fig. 5. The linear regression fits for the *hull* sites in Fig. 5 indicate the slopes of about 0.922 for ordinary percolation and 0.914 for fully coordinated percolation with essentially perfect fits, again reinforcing the conclusion that they show the same *static* critical behavior.

V. SUMMARY AND CONCLUSION

In summary, we have studied both static and dynamic critical behaviors associated with a model of the highly connected regions of a disordered cluster. The model is a *site* variant of the four-coordinated percolation [2,3] on the square lattice we call *fully coordinated percolation*. While the bond version was studied for *static* critical behavior, neither bond nor site version was previously studied for the dynamic behavior to the best of our knowledge. We have used various methods such as Monte Carlo simulations, finite-size scaling and Arnoldi-Saad approximate diagonalization of large random matrices for this purpose.

Though all indications are that the static behavior of this model is exactly the same as the ordinary percolation (as previous work suggested), the dynamic behavior shows a small but significant difference in the values of the universal critical exponents. We have looked for the cause of this difference and found a threefold increase in the number and significantly enhanced clustering of the interior sites (i.e., those not on the exterior or internal boundaries) and the associated decrease in the number of boundary sites. Thus, although the deviations from ordinary percolation in terms of the values of the dynamic critical exponents are not large, there will be rather significant differences in any processes that depend sensitively on those numbers. Possible examples of such processes include the oxidation of a material through the external embedding phase and the vibrational normal modes with boundary conditions such as *clamping* or *tethering* of the external boundaries (through the contrast in elastic constants of embedding and embedded materials, for example).

ACKNOWLEDGMENTS

One of us (J.H.K.) wishes to thank the Purdue University Department of Physics for their hospitality and Kangnung National University for their financial support during his visit to Purdue University where part of the work was done. We are also grateful to D. Stauffer and R. Ziff for insightful remarks.

[1] D. Stauffer and A. Aharony, *Introduction to Percolation Theory*, revised 2nd ed. (Taylor and Francis, London, 1994).
[2] R.L. Blumberg, G. Shlifer and H.E. Stanley, J. Phys. A **13**, L147 (1980).
[3] A.E. Gonzalez and P.J. Reynolds, Phys. Lett. **80A**, 357 (1980).
[4] J. Adler, Physica A **171**, 453 (1991).
[5] S. Mukherjee and H. Nakanishi, Fractals **4**, 273 (1996).
[6] S. Mukherjee and H. Nakanishi (Private communication).

[7] V. Privman, P. C. Hohenberg, and A. Aharony, in *Phase Transitions and Critical Phenomena*, edited by C. Domb and J.L. Lebowitz (Academic, London, 1991), Vol. 14.

[8] H. Nakanishi, in *Annual Reviews of Computational Physics*, edited by D. Stauffer (World Scientific, Singapore, 1994), Vol. 1.

[9] S. Mukherjee, H. Nakanishi, and N.H. Fuchs, Phys. Rev. E **49**, 5032 (1994).

[10] S. Alexander and R. Orbach, J. Phys. Lett. **43**, L625 (1982).

[11] S. Mukherjee, D.J. Jacobs, and H. Nakanishi, J. Phys. A **28**, 291 (1995).